

THE EFFECT OF LEG DESIGN ON ROBOTIC RUNNING GAITS

NSF Summer Undergraduate Fellowship in Sensor Technologies 2007

Nataliya Kilevskaya - University of Florida

Advisors: Dr. Clark and Kevin Galloway

ABSTRACT

Advances in legged robotics have led to the development of robots capable of running over rough terrain. Edubot, one such hexapedal robot, is a biologically inspired runner that mimics the cockroach in its alternating tripod gait and compliant legs. Most animals' running gaits can be approximated by the Spring-Loaded Inverted Pendulum (SLIP) model, which treats an animal as a point mass on a linear spring. The SLIP model has been demonstrated to accurately model the center of mass motion of running animals, as well as the ground reaction forces associated with their gaits. While Edubot's running behavior can also be viewed in terms of the SLIP model, the linear spring in the model fails to capture the complexity of the compliant C-shaped legs of the robot. These legs have shown superior performance over all previous designs. In this paper we attempt to isolate the characteristics of the C-legs and study their individual and combined effect on performance in hopes of understanding how to design better legs. We do this by decoupling and mathematically modeling the spring rest length and the effective stiffness of the leg as it rolls through stance. Using a SLIP model modified with our equations, we show evidence that both a decreasing stiffness and an increasing spring rest length during stance are important contributors to performance. We then describe legs designed to test our model's predictions.

CONTENTS

| | |
|--|-----------|
| 1 INTRODUCTION | 3 |
| 2 BACKGROUND | 4 |
| 2.1 SLIP MODEL FOR ANIMAL RUNNING | 4 |
| 2.2 PSUEDO RIGID BODY MODEL FOR C-LEG | 6 |
| 3 OVERVIEW OF MODELING | 6 |
| 4 CONSERVATIVE SLIP MODEL | 7 |
| 5 NONCONSERVATIVE SLIP MODEL | 8 |
| 6 MODELING C-LEG SPECIFIC CHARACTERISTICS | 9 |
| 6.1 INCREASING SPRING REST LENGTH | 10 |
| 6.2 DECREASING STIFFNESS | 11 |
| 6.3 TANGENTIAL DEFLECTION COUPLING | 13 |
| 7 DESIGNING LEGS | 14 |
| 8 RESULTS | 14 |
| 9 DISCUSSION | 15 |
| 10 RECOMMENDATIONS | 16 |
| 11 ACKNOWLEDGEMENTS | 16 |
| 12 REFERENCES | 16 |
| APPENDIX A | 18 |

1. INTRODUCTION

Research in the field of robotic legged locomotion aims toward the development of robots that are capable of stable, speedy, and energetically efficient locomotion over a variety of terrains. As these characteristics are readily demonstrated in animal locomotion, researchers have increasingly turned to biological studies for design inspiration. The cockroach, which demonstrates static and dynamic stability and is capable of running at speeds up to 50 body-lengths per second [1], has served as a template for numerous robots, including the Ajax [2], RHex[3], and Sprawlita [4] platforms.

Analysis of animal locomotion has demonstrated that during energetic gaits, such as running and hopping, animal legs behave as springs, storing and releasing energy during ground contact. This spring-like behavior is provided by the joint action of muscles, ligaments, and tendons undergoing compression and tension [5]. To mimic this biological behavior, researchers have introduced legs made partly or fully from compliant materials. These compliant limbs deflect under load, acting like springs and contributing to the overall stability of the robot by absorbing shock due to impacts [6]. The RHex robot platform, developed at the University of Michigan and McGill University, takes full advantage of this mechanism. It employs six compliant legs and uses an alternating tripod gait, with the front and back legs on each side synchronized with the middle leg on the other side, to achieve speeds of over 5 body length per second over uneven terrain [7].

Dr. Koditschek's laboratory at the University of Pennsylvania largely works with Edubot, a robot of the RHex family. The legs on Edubot are currently a compliant half-circle produced by Shape Deposition Manufacturing (SDM) and pictured in *Figure 1*.

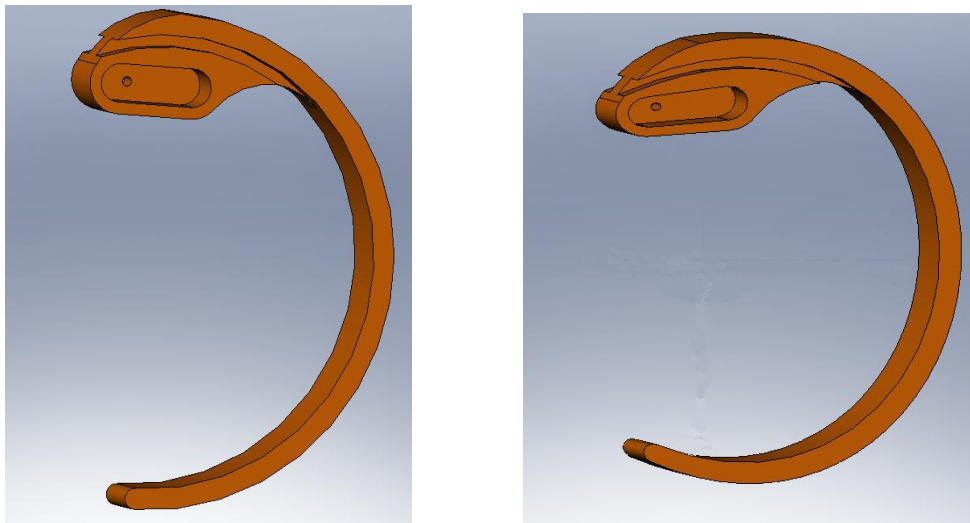


Figure 1: (left) undeflected C-leg, (right) deflected C-leg.

These C-shaped legs have been very effective in improving the efficiency, speed, and mobility of the RHex family with respect to previous iterations. For example, the geometry of the C-leg has led to a 37% decrease in power requirements during stair climbing, as compared to the previous four-bar linkage legs [8]. Other multi-legged robotic platforms have experimented with different leg geometries. Raibert's quadruped robots used straight legs with air springs, to provide compliance, and actuators, to change each leg's length. These robots were successful in balancing to achieve a running gait on a flat surface, but did not exhibit the passive stability necessary for rough terrain traversal [9]. Motivated by a desire to understand the C-leg's superior performance and to design legs that will further improve Edubot's locomotion, we have noted the four essential features exhibited by the C-leg geometry that are not present in the straight leg:

- i. Due to the rolling point of contact during stance, the effective leg length increases as stance progresses.
- ii. The radial stiffness decreases during stance
- iii. The C-leg demonstrates tangential deflection under load, as opposed to simply radial deflection, due to the coupling of motion in the tangential and radial directions inherent in the C- geometry. The radial direction is defined as toward the hip joint, while the tangential direction is that perpendicular to it in the sagittal plane.
- iv. As the leg rolls through stance, the point of largest deflection on the leg, or the virtual pivot, moves slightly down the leg.

Our goal is to learn which factors are responsible for the superior performance demonstrated by the C-leg. Is it simply the lift provided during stance to the robot's center of mass by the passive increase in the effective leg length or does the coupling of deflection in the radial and tangential directions play a role? To answer this and other questions we aimed to create a simple and abstracted SLIP-like model of Edubot's motion that incorporated the unique features due to the C-leg's geometry discussed above. By then independently activating and deactivating the various factors within the model, we would be able to separate and analyze their respective effects on performance. These theoretical results can then be tested empirically by the construction of legs that isolate the different features of the C-leg in their alternative geometry. By running Edubot with the modified legs, we would learn whether our model accurately captures the dynamics of the C-leg and the robot and would identify features advantageous to future leg design.

2 BACKGROUND

2.1. Spring Loaded Inverted Pendulum Model for Animal Running

To develop a model for Edubot's motion, we built on the previous work done in modeling trotting, running, and hopping in animals. The Spring- Loaded Inverted Pendulum model (SLIP) has successfully approximated the sagittal plane dynamics and ground reaction forces of animals ranging from cockroaches to kangaroos [10]. This model treats an animal or robot as a point mass on a single mass-less linear spring as

demonstrated in *Figure 2*, with the forward motion of the center of mass of an animal being modeled by the spring-mass system in two independent stages: the flight stage and the stance stage. During the flight stage, the motion is dictated by the effect of gravity on the mass. The stance phase occurs from the moment the spring-leg comes in contact with the ground at some angle, through its compression, rotation and decompression, and until it leaves the ground at its full length. During the stance phase, the opposing forces responsible for the spring's compression and eventual decompression are gravity and the spring force. The effect of gravity is directly dependent on the mass, while the spring force is directly proportional to the compression of the spring. The specific trajectory followed by the SLIP model is dependent on the angle of incidence of the spring with the vertical upon touchdown and the vector of the landing velocity of the center of mass [10].

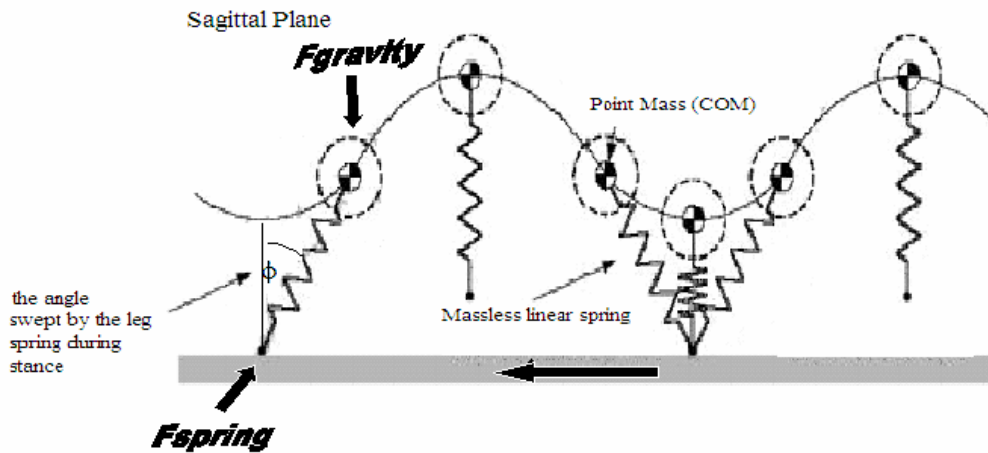


Figure 2: SLIP model of animal running. During the flight phase, gravity determines the dynamics of the mass. During the stance phase, the force of the spring opposes the force of gravity –adapted from [11].

While the model appears to assume a monopod, or a bipedal gait in which both legs are never on the ground simultaneously, it accurately describes bipedal, quadruped, and hexapod dynamics with the introduction of Sutherland's virtual leg [12]. Here a virtual leg describes the idea that legs whose motion is synchronized can be modeled as a single leg. In a hexapod, the three legs comprising a single tripod are synchronized, resulting in two virtual legs. Similarly, quadrupeds can be treated as bipeds. Since the two virtual legs are never both in stance, we are justified in treating them as we would those of a bounding monopod [10].

Given that Edubot was largely biologically inspired, the SLIP model of motion is a valid candidate to capture the dynamics of its center of mass, with the stiffness of the three legs of a tripod determining the spring constant of the single linear spring that represents the virtual leg in the model. In fact Altendorfer, et al.[13] previously introduced a clock-driven SLIP model to describe RHex's dynamics in the sagittal plane.

2.2 Psuedo Rigid Body Model for C-leg

The standard SLIP model, although successful in describing RHex's general dynamics, fails to address the variation caused by the C-leg geometry. As formerly mentioned, the C-leg exhibits characteristics of a non-linear spring. It has been modeled by two orthogonal linear springs which simplify the C-shape to a sideways 'V', but retain the tangential, as well as the radial, deflection under load [14]. More recently, the C-leg has been simplified using a pseudo-rigid-body analysis [15] to a rigid leg-link attached to the hip joint by a torsional spring at the effective center of rotation, or the characteristic pivot, as illustrated in *Figure 3*. The effective leg stiffness is captured in the spring constant of the torsional spring and the model preserves the deflection coupling in the radial and tangential directions. Moreover the model can accommodate the change in stiffness and leg length of the C-leg during roll by changing the length of the rigid leg-link as a function of the leg angle [16]. Prior analysis of RHex's motion has always focused on the control of the leg, and ignored its geometry. Modeling of the C-leg has largely ignored its dynamic interaction with the robot body. Our goal is to create a model which takes both the dynamics of the center of mass of the robot and the geometry of the C-leg into account.

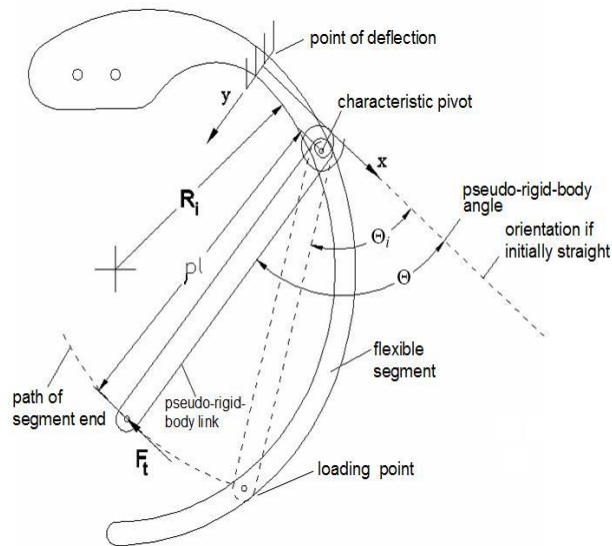


Figure 3: Psuedo rigid body model of the C-leg. The C-leg can be approximated by a rigid leg-link attached to the hip joint by a torsional spring –adapted from [16].

3 OVERVIEW OF MODELING

To create our model for Edubot's motion based on the C-leg geometry, we use a method of increasing complexity at each stage. We begin by modeling Edubot as a simple SLIP model, and seek to find stable gaits that are characteristic of Edubot's motion. We then add damping and energy addition to the model, and observe the effects on the system.

Once we have a stable system, we add the specific characteristics associated with the geometry and material of the C-leg. We are then free to manipulate these characteristics to isolate their effect on performance.

The simulation of our mathematical models is achieved through the use of MATLAB v7. Specifically the differential equations involved in the equations of motion of our simplified models are solved numerically using the ode45 solver function. Ode45 is a variable step differential equation solver that employs the Runge-Kutta formula [17].

4 CONSERVATIVE SLIP MODEL

Due to the SLIP model's success in describing animal running, it seems only natural to start by approximating Edubot's motion in the sagittal plane with a SLIP model tuned to Edubot's physical parameters and that demonstrates a gait characteristic of the robot. Our initial model is conservative. It does not account for the energy loss due to friction, and therefore requires no energy addition to compensate. The equations of motion are derived from a straightforward force analysis. During flight, the system is governed by gravity,

$$\begin{aligned}\ddot{x} &= 0, \\ \ddot{y} &= g,\end{aligned}\tag{1}$$

where (x,y) are respectively the horizontal and vertical displacement from the origin and g is -9.8 m/s^2 , the gravitational constant. During stance, the force of the spring contributes to the dynamics of the system. Since this force always acts along the direction of the spring, we add a polar component for ease of analysis.

$$\begin{aligned}\ddot{x} &= \frac{k}{M}(l_0 - r)\sin\theta, \\ \ddot{y} &= g + \frac{k}{M}(l_0 - r)\cos\theta.\end{aligned}\tag{2}$$

Here k , M , and l_0 are the spring stiffness, mass, and rest length respectively, and are parameters of the spring-mass system. Conversely, (r, θ) are determined by the state variables of the system, where r is the distance from a local origin and θ is the angle with the vertical, with a range of $[-\theta_0, \theta_0]$, where θ_0 is the angle of incidence with the vertical at touchdown. The local origin is the current point of touchdown of the spring, around which it pivots during stance.

With our equations of motion derived, we turn to tuning them to a characteristic running gait for Edubot. First, θ_0 must correlate to the angle swept by the C-leg during stance. We restrict this angle to fall in the range of [20,50] degrees to maintain physical justification. Second, we set M , the mass in our model, to 2.69 kg, the experimentally measured weight of the robot. Since, Edubot demonstrates a variety of stable running trajectories, it is important that our SLIP model act in a similarly stable matter, with its horizontal velocity returning to the same value on subsequent liftoffs. The SLIP equations are inherently unstable, with most trajectories resulting in an eventual collapse of the system. To minimize the instability of the system, we fix θ_0 to a constant for every

touchdown. While this eliminates variable touchdown angle as a source of added complexity, the system remains unstable for most trajectories. To correlate with the stable behavior exhibited by Edubot, our sole interest lies in stable equilibrium gaits. To find these we turn to stability analysis of dynamical systems, by using the Poincare Map approach.

Poincare Maps reduce continuous systems to discrete systems by turning an n dimensional state space into an $n-1$ dimensional one. The problem of finding a periodic orbit of a differential equation then reduces to the problem of finding a fixed point on a map. By choosing an appropriate Poincare section we can then find equilibrium gaits by identifying fixed points in the section. In order to construct a Poincare Map we require a closed form solution of our equations of motion. Since the SLIP equations cannot be solved explicitly, we turn to searching numerically for fixed points. We use a vector field approach as detailed in [18]. Choosing the beginning of stance, or touchdown, as our Poincare section, we search a mesh of touchdown angle and velocity initial conditions for fixed points. Our search is unsuccessful in finding any stable equilibriums; consequently we turn to a non-conservative SLIP model.

5 NONCONSERVATIVE SLIP MODEL

Failing to find stable equilibrium trajectories for a conservative SLIP model, we turn to a model that includes energy dissipation and addition. Our hope is that the addition of damping into the system will introduce stability for a range of initial starting conditions. We model the dissipative effects of friction by adding a damper in parallel with the spring. The damper acts in the direction opposing v , the velocity of our mass, with it exerting a force F_d determined by

$$F_d = -bv, \quad (3)$$

where b is the damping coefficient. To keep the system from rapidly approaching rest, we need to provide a method for adding energy into the model. One strategy, implemented in [18] and [19], is to temporarily increase the spring constant at the moment of max compression and then reset it upon take off. This instantaneously increases the amount of energy stored in the system. Unfortunately this method has no physical basis. Instead, we choose to add energy into the system by fixing the angular velocity, $\dot{\phi}$, of the spring during stance. Since Edubot uses motors to rotate its legs, this scheme attempts to approximate the way these motors add energy into the system. In a physical system, motors are controlled by a proportional derivative (PD) controller which attempts to maintain a constant angular velocity by regulating the torque output of the motors. Since realistically PD tracking cannot retain a constant angular velocity, our assumption of a constant $\dot{\phi}$ is a simplification based on an ideal PD controller. While this will inevitably lead to discrepancies between the experimental and simulated behavior, this energy addition scheme seems to be the most physically relevant. In addition, it simplifies the model by reducing the effect of the dynamics on the system. While the flight dynamics continue to be governed by eq.1, our damped model is best described completely in polar coordinates during the stance phase,

$$\begin{aligned}\dot{\varphi} &= C_1, \\ \ddot{r} &= g \cos \varphi + \frac{k}{M}(l_0 - r) - \frac{b\dot{r}}{M},\end{aligned}\tag{4}$$

where φ is the angle of the spring with the vertical and r is the instantaneous length of the spring. This polar coordinate system functions only as a local coordinate system and must be converted to the global rectangular coordinates for every flight phase.

Figure 4 shows a plot of the horizontal and vertical trajectories of the non-conservative model with sample initial conditions and parameters that are close approximations of Edubot. Both the horizontal and vertical trajectories settle into a stable equilibrium gait after a short period of time. Simulations using a variety of initial conditions have shown that the system stabilizes for a wide range of gaits. With a wide base of stable gaits to choose from, we have no need to numerically search out equilibrium gaits as with the conservative model. We now turn our attention to modifying our model to incorporate the unique characteristics of the C-leg.

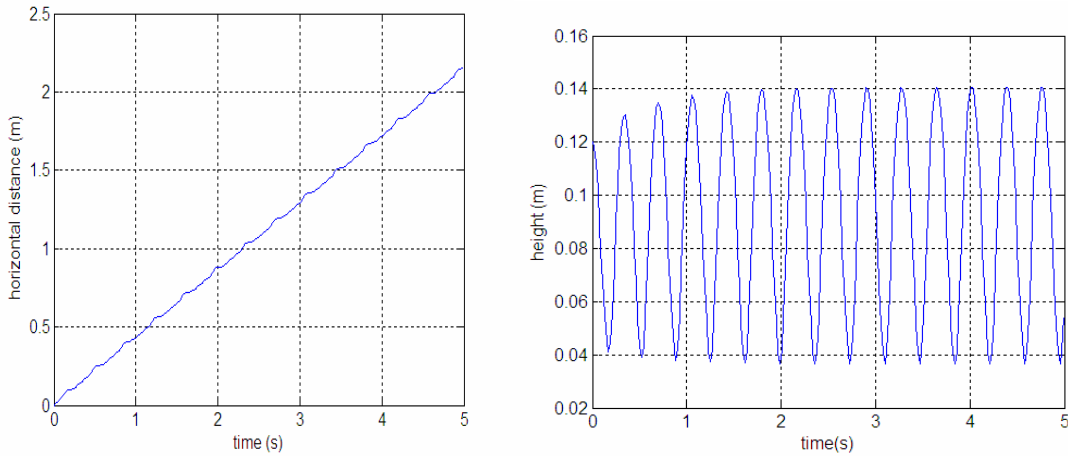


Figure 4: (left) simulated horizontal trajectory, (right) simulated vertical trajectory. Note: both quickly arrive at a steady state.

6 MODELING C-LEG SPECIFIC CHARACTERISTICS

To understand the effect of individual leg design characteristics on performance, we wish to mathematically isolate them and work them into a comprehensive model for Edubot's running, where we can then selectively activate them to explore their effect. As previously mentioned, some of the C-leg differences from a linear spring include an increase in spring rest length and a decrease in effective stiffness as the leg rolls through stance. Here the effective stiffness is the stiffness in the radial direction, from the loading point of the leg to the hip. Using our non-conservative model as a base, we aim to map

the non-linear changes in stiffness and spring rest length onto a SLIP-like model with a one-dimensional spring as demonstrated in *Figure 5*. For this we must develop equations for l_0 and k , based on the C-leg geometry and material properties, to substitute into eq. 4.

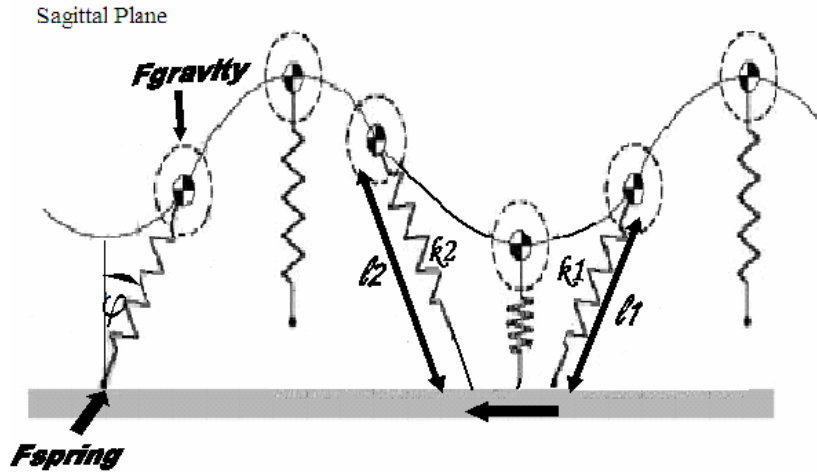


Figure 5: SLIP model of animal running modified to include C-leg properties. Spring rest length increases during stance: $l_2 > l_1$. Stiffness decreases over stance: $k_1 > k_2$. The horizontal displacement during stance due to the roll is modeled by the spring end slipping along the ground at a constant velocity – adapted from [11].

6.1 Increasing Spring Rest Length

Figure 6 illustrates the mapping between the undeflected C-leg and a one-dimensional spring. It is clear that the spring rest length, l_0 , changes during stance and is dependent on r_l , the radius of the half-circle C-leg, and φ , the instantaneous angle with the vertical of the virtual radial spring stretching from the hip to the loading point. Since r_l is a constant for any particular C-leg, l_0 can be written as a function of φ , which changes in stance according to eq. 4. A geometric analysis of *Figure 6* yields

$$l_0 = 2r_l \cos \varphi. \quad (5)$$

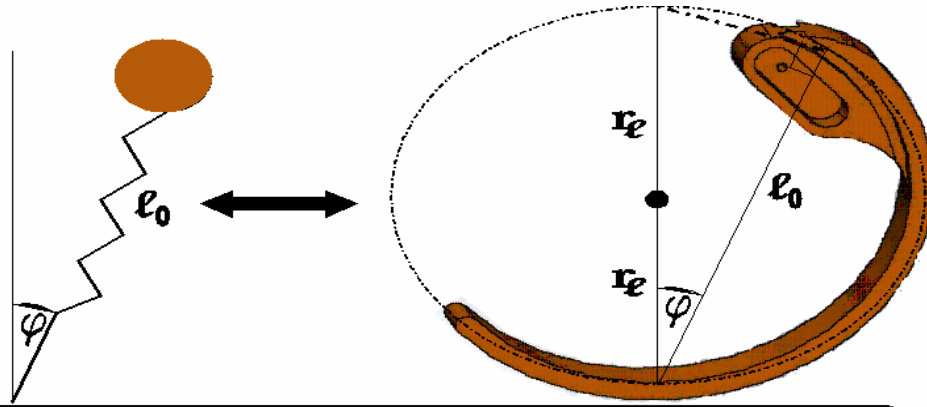


Figure 6: Physical mapping between C-leg and a one-dimensional spring.

6.2 Decreasing Stiffness

To approach the problem of mathematically characterizing the changing stiffness during stance, we turn to the pseudo rigid body model of the C-leg. From this model, we can intuitively see why the effective stiffness of the leg decreases as it rolls through stance. During stance the loading point moves further away from the characteristic pivot, thereby increasing n , the length of the moment arm, as shown in *Figure 7*. An increase in n results in a larger torque being applied to the torsional spring for the same amount of force. This translates to an increased deflection per Newton, or a less stiff effective radial spring. This virtual radial spring is illustrated in *Figure 7* in both a deflected and undeflected position.

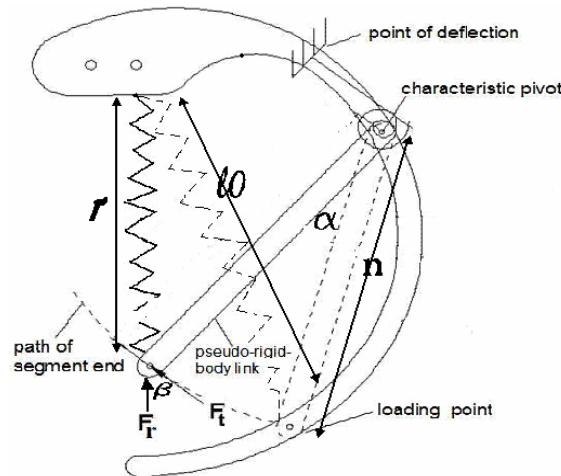


Figure 7: Pseudo rigid body model of C-leg illustrating the behavior of the virtual radial spring during compression. Adapted from [16].

If we impose Hooke's law on this spring,

$$F_r = k(l_0 - r), \quad (6)$$

where F_r is the component of the ground reaction force acting along the line of the radial spring, then we can solve for k , the effective radial stiffness as a function of F_r and the difference between the spring's current length and its rest length. At this point we require an expression for F_r in terms of known states. The angular form of Hooke's law tells us that

$$F_t n = k_t \alpha, \quad (7)$$

where F_t is the component of the ground reaction force acting perpendicular to the moment arm, k_t is the torsional spring constant, and α is the angle of twist in radians. At this point we make the approximation that

$$F_t = F_r \cos \beta, \quad (8)$$

where β is the angle between the two force vectors. The accuracy of this approximation depends on the angle of the leg with the ground, and subsequently the angle of the ground reaction force vector. A larger angle between the ground reaction force and F_r corresponds to a larger error in the approximation.

Using eqs. 6, 7, and 8, we find that

$$k = \frac{k_t \alpha}{n(l_0 - r) \cos \beta}. \quad (9)$$

Using geometry α , n , and β can be expressed in terms of r_t , l_0 , r , and d , the arc length between the hip and the point of deflection. These expressions and their derivations are detailed in Appendix A. The torsional spring constant, k_t , is given by

$$k_t = \rho K_\ominus \frac{EI}{h}, \quad (10)$$

where I is the moment of inertia, E is the Young's modulus of the C-leg epoxy, h is the arc length from the point of deflection to the loading point, K_\ominus is the stiffness coefficient, and ρ is the characteristic radius factor. Both K_\ominus and ρ can be approximated from the ratio of h and r_t as demonstrated in a look-up table in [15].

We now have an expression for k , the effective radial stiffness, which incorporates the material characteristics and geometry for a give C-leg. *Figure 8* demonstrates the relationship between our analytical k and an experimentally measured k derived from data collected for another experiment [16]. The experimental k was determined by using a force plate and measuring the radial deflection for a given force. The two curves demonstrate the same shape, which suggests that our equation has captured some fundamental behavior of the radial stiffness. Nevertheless, there is a large build-up of error for the later data points. This is most likely attributed to our force relationship approximation. It may be possible to correct for this error, but first more force data need to be taken to further study the correlation between the analytical and experimental k . Specifically, data collected from a single C-leg at various loading points and for various

degrees of deflection would be the most effective for identifying and rectifying the cause of error.

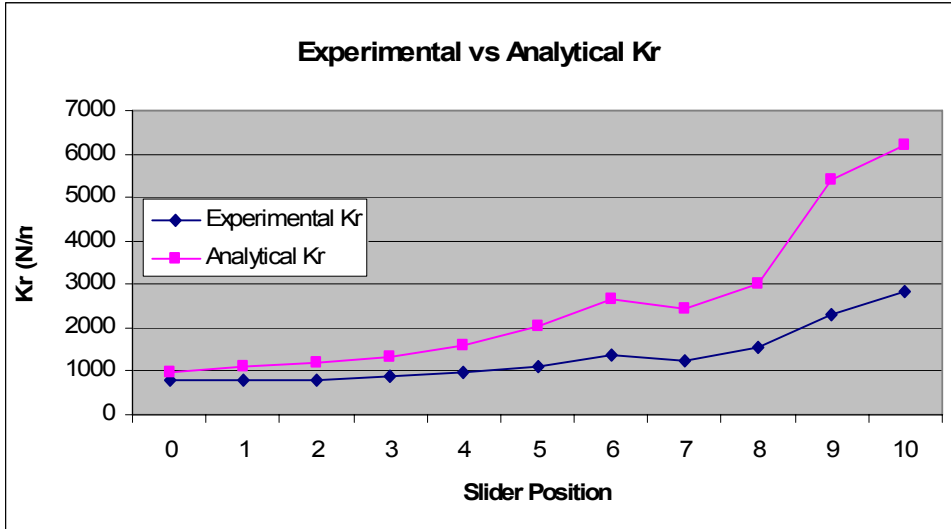


Figure 8: Graph showing the correlation between the experimental and analytical radial stiffness. Experimental data was gathered using a force plate and measuring radial deflection for a given force. The Slider Position refers to a variable stiffness C-leg and corresponds to different locations for the point of deflection. Larger slider numbers indicate a point of deflection further from the hip.

Since at this point we do not have an accurate analytical expression for k , we turn to using a temporary equation,

$$k = k_0 \cos(C_2(\varphi_0 + \varphi)), \tag{11}$$

where k_0 is our initial radial stiffness upon touchdown, C_2 is a constant chosen to best capture the rate at which stiffness decreases for a particular C-leg, φ_0 is the touchdown angle with the vertical and φ is initialized at $-\varphi_0$. While this equation fails to capture the exact relationship between the geometry of the C-leg and its changing radial stiffness, it captures the overall trend of a non-linear decrease in stiffness as Edubot progresses through stance, or as φ increases. This is sufficient for our purpose of determining how changing stiffness affects performance, but inadequate for tuning the model to specific C-legs determined by their material and point of deflection.

6.3 Tangential Deflection Coupling

While our initial goal included mathematically characterizing the tangential deflection of the C-leg and including it in our model, the task proved too complex for the summer. Our model therefore makes no attempt to include the coupling of deflection in the radial and tangential directions, choosing to concentrate, for the time being, on the other characteristics that distinguish the C-leg.

7 DESIGNING LEGS

With a preliminary mathematical model determined, we now turn to the task of empirically testing its predictions. For this we require leg designs that isolate our characteristics of interest. *Figure 9a* is an illustration of a leg which demonstrates a decreasing radial stiffness but maintains the spring rest length at a constant during stance. The leg pictured in *Figure 9b* includes both decreasing stiffness and increasing rest length. The point of deflection is further down the centroidal axis than on the current C-legs as an attempt to minimize the tangential deflection, which is not captured in our current model. Currently, the first iteration of the leg in *Figure 9b* has been constructed using SDM, as shown in *Figure 9c*, but has yet to be tested on Edubot.

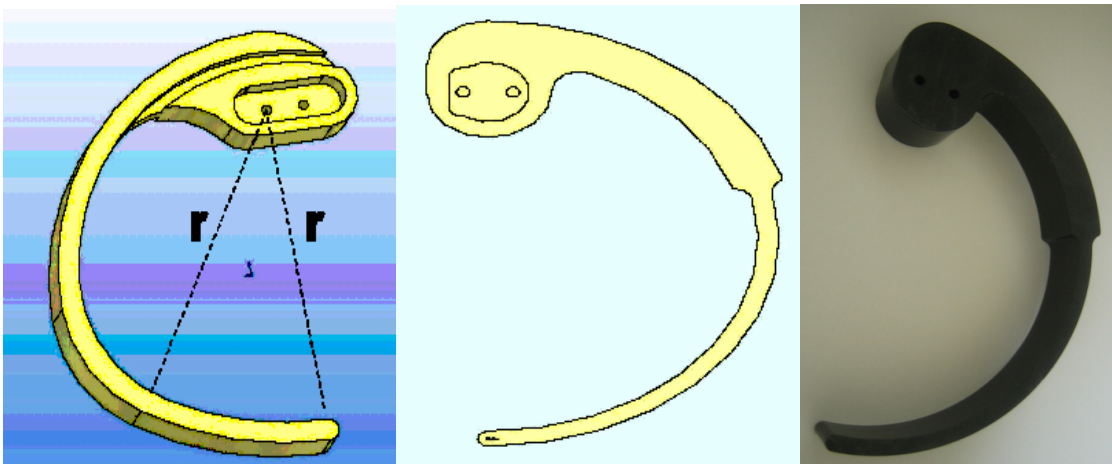


Figure 9: (left) a. Leg design with decreasing radial stiffness but constant spring rest length. (middle) b. Leg design with decreasing radial stiffness and increasing spring rest length. (right) c. First iteration of leg with decreasing radial stiffness and increasing spring rest length.

8 RESULTS

Using our non-conservative modified SLIP model, we ran simulations of several different leg designs for velocity and maximum height at steady-state. Ideally we want to measure performance in terms of velocity, energetics, and stability, but due to time restrictions our performance metrics are maximum height, which we intuitively correlate with stability, and velocity. Our models included a straight linear spring leg for comparison, a leg with increasing spring rest length, a leg with decreasing stiffness, and a leg incorporating both. *Figure 10* captures these results as a comparison.

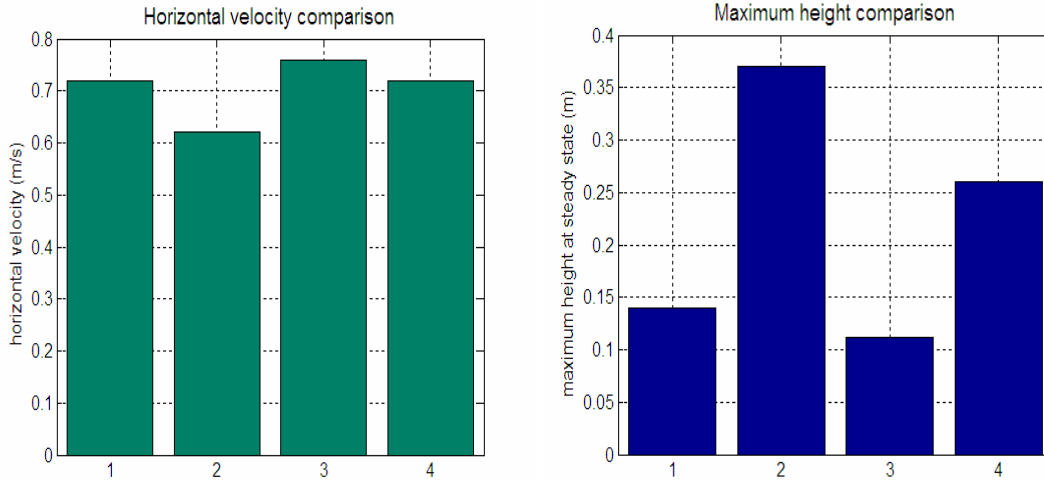


Figure 10: (left) a. Comparison of horizontal velocities at steady state for different models. (right) b. Comparison of maximum height at steady state for different models. (1) corresponds to a straight, linear spring leg, (2) to a leg with increasing spring rest length, (3) to a leg with decreasing radial stiffness, and (4) to a leg with both properties.

Figure 10a demonstrates that horizontal velocity is hampered by simply increasing the spring rest length during stance, but aided by adding decreasing radial stiffness. Figure 10b demonstrates that increasing spring rest length correlates with an increase in maximum height, while decreasing stiffness corresponds to a decrease. When both characteristics are present, the effect of the increasing spring rest length appears to dominate, resulting in an increase in maximum height with respect to our base comparison, the linear spring leg. Using the approximation that greater maximum height corresponds to greater stability when our initial maximum height is only slightly larger than the spring length, we draw the following preliminary conclusions: A decreasing k affects performance by increasing velocity and decreasing stability. An increasing l_0 affects performance in the exact opposite manner. The presence of both results in increased stability, and has no significant effect on velocity.

9 DISCUSSION

While our results suggest that including both an increasing spring rest length and a decreasing radial stiffness improve performance, several factors need to be considered before making any concrete conclusions. Our simulation used a gait judged to be characteristic of Edubot's motion:

$$M = 2.69\text{kg}, r_l = .0675\text{m}, k_0 = 1400 \frac{\text{N}}{\text{m}}, \varphi_0 = \frac{2\pi}{9}, \dot{\varphi} = 4.19 \frac{\text{rad}}{\text{s}}, \dot{x}_0 = .5 \frac{\text{m}}{\text{s}}.$$

Although this is a valid preliminary approach, we further need to run an optimization for each individual model and compare their optimized gaits.

The main contribution of this work is the development of a framework for a SLIP-like model of Edubot's running that includes the unique properties of the C-leg. Using this framework, future work can verify our model's prediction that both decreasing stiffness and increasing spring rest length contribute to the C-leg's success. This could inform the design of legs and ultimately lead to better legs for Edubot, and legged robots in general, with an increase in its overall performance.

10 RECOMMENDATIONS

In this work we attempted to mathematically characterize the unique characteristics of the C-leg, but were unable to create a comprehensive analysis in our allotted time frame. Future work should focus on incorporating tangential coupling into the model. In addition, our pseudo rigid body based equation for stiffness shows promise in predicting the effective radial stiffness for a variety of C-legs. Work focused on reconciling the equation to experimental results would be very useful in determining the best material to use and the optimal location for the point of deflection in future C-legs.

11 ACKNOWLEDGEMENTS

I would like to thank my advisors, Dr. Jonathan Clark and Kevin Galloway, for all their time and help in my project this summer. In addition, I would like to thank Dr. Koditschek for giving me the opportunity to work in his lab this summer. It was a very educational experience. I am also grateful to all my colleagues in KodLab for their assistance, especially Goran Lynch, for his insights, and Viktor Orekhov, for his help in building legs. I would also like to thank the SUNFEST program, NSF REU, and Dr. Van der Spiegel for all his efforts.

12 REFERENCES

- [1] Full, R.J., and Tu, M.S., "Mechanics of a Rapid Running Insect: Two-, Four-, and Six-legged Locomotion," *J. of Experimental Biology*, v 156, 1991, p 215-231,.
- [2] Kingsley, D.A., Quinn, R.D., Ritzmann, R.E., "A cockroach inspired robot with artificial muscles," presented at *IEEE/RSJ Int. Conf. on Intelligent Robots and Systems*, Beijing, China, Oct. 2006.
- [3] Saranli, U., Buehler M., and Koditschek, D., "RHex: A simple and highly mobile hexapod robot," *Int. J. of Robotics Research*, v 20, n 7, July 2001, p 616-31,.
- [4] Cham, J.G., Bailey S., Clark J.E., et al., "Fast and Robust: Hexapedal Robots via Shape Deposition Manufacturing," *Int.l J. of Robotics Research*, v 21, n 10-11, Oct.-Nov. 2002, p 869-82.

- [5] Alexander, R.M., *Elastic Mechanisms in Animal Movement*. Cambridge, UK: Cambridge Univ. Press, 1988.
- [6] Brown, H.B., Raibert, M.H. “Legs that deform elastically,” *Proc. Sixth CISM-IFTOMM Symposium on Theory and Practice of Robots and Manipulators*, Cracow, Poland, 1987, p 436-43.
- [7] Weingarten, J.D., Lopes, G.A.D., et al., “Automated gait adaptation for legged robots,” *Proc. IEEE Int. Conf. on Robotics and Automatgion*, v3, 2004, p 2153-2158.
- [8] Moore, E.Z., Campbell D. , et al., “Reliable Stair Climbing in the Simple Hexapod ‘RHex,’” *Proc. IEEE Int. Conf. on Robotics and Automation*, v 3, 2002, p 2222-2227.
- [9] Raibert, M.H., et al. “Running on four legs as though they were one,” *IEEE J. of Robotics and Automation*, v RA-2, n 2, Jun. 1986, p 70-82.
- [10] Blickhan, R., Full, R.J., “Similarity in multilegged locomotion: Bounding like a monopode,” *J. of Comparative Physiology*, v A, n 173, 1993, p 509-517.
- [11] Sato, A., (c 2002-2005), http://www.cim.mcgill.ca/~aki/research/SLIP_Hopper.htm.
- [12] Sutherland, I.E., Ullner, M.K., “Footprints in the Asphalt,” *Int. J. of Robotics Research*, v 3, n 2, 1984, p 29-36.
- [13] Altendorfer, R., Koditschek, D.E., Holmes, P., “Stability analysis of a clock-driven rigid-body SLIP model for RHex,” *Int. J. of Robotics Research*, v 23, n 10-11, Oct./Nov., 2004, p 1001-1012.
- [14] Lin, P.C., “Proprioceptive sensing for a legged robot”. PhD thesis, University of Michigan. 2005.
- [15] Howell, L.L., *Compliant Mechanisms*. Wiley, New York. 2001.
- [16] Galloway K.C., et al., “Design of a Multi-Directional variable stiffness leg for dynamic running,” unpublished.
- [17] The MathWorks Inc., Matlab, (c 1994-2006), <http://www.mathworks.com/>.
- [18] Burden, S., “The role of leg differentiation in hexapedal running,” SUNFEST REU Final Report. 2006.
- [19] Buehler, M. and Koditschek, D.E., “Analysis of a simplified hopping robot,” *International J. of Robotics Research*, v 10, n 6, 1991, p 587–605.

APPENDIX A

We derive expressions for α , n , and β by geometrically analyzing the C-leg as a half circle. *Figure 11* provides an illustration of our geometric model.

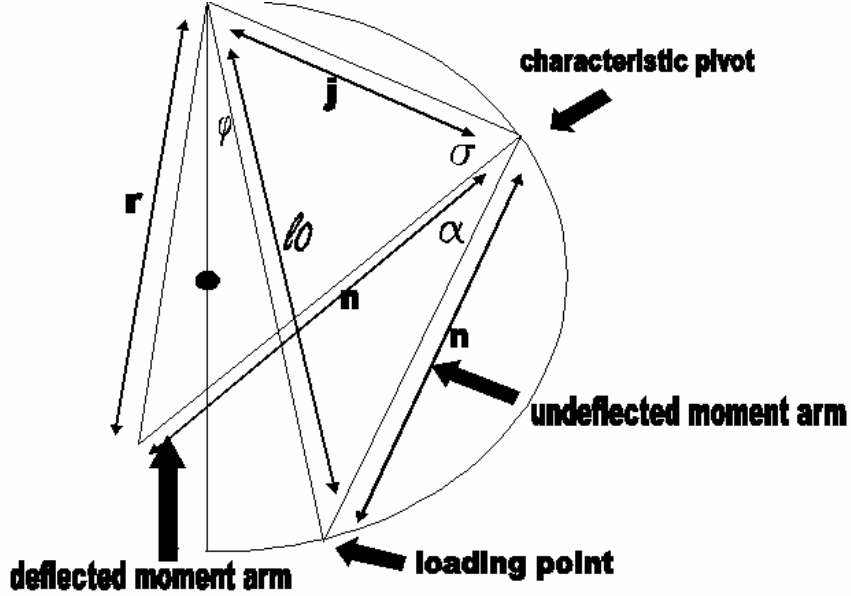


Figure 11: The C-leg as a half-circle. n represents the length of the moment arm and r represents the effective radial length of the spring after deflection.

From it we can extract by inspection that

$$\alpha = \frac{\pi}{2} + \varphi - \sigma. \quad (12)$$

φ can be determined from l_0 as we have previously established, but we still need an expression for σ . Using the Law of Cosines on the triangle determined by r , j , and n , we find that

$$r^2 = j^2 + n^2 - 2jn \cos \sigma. \quad (13)$$

The unknowns in this equation are j and n . We begin by finding an expression for j . *Figure 12* provides the necessary geometry for that analysis. Using the Law of Sines we find that

$$j = \frac{r_l \sin \kappa}{\sin(\frac{\pi - \kappa}{2})}, \quad (14)$$

where κ can be determined using the relationship between an arc length and its corresponding arc angle such that

$$\kappa = \frac{d + p}{r_l}. \quad (15)$$

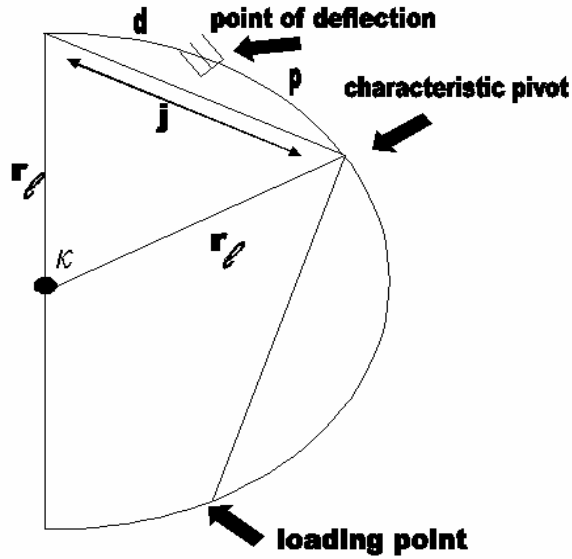


Figure 12: The C-leg as a half-circle with the secants that are relevant to finding j shown. d is the arc length between the hip and the point of deflection and p is the arc length between the point of deflection and the characteristic pivot.

While d is a known parameter, we approximate p , the arc length between the point of deflection and the characteristic pivot, by

$$p = (1 - \rho)(S - d), \quad (16)$$

as detailed in [13]. Here ρ is the characteristic radius factor and S is the total arc length between the hip and the loading point and can be expressed as

$$S = r_l(\pi - 2\varphi). \quad (17)$$

We have now derived an expression for j in terms of known variables. We now turn to finding an expression for n . *Figure 13* reveals that using the Law of Sines we can find that

$$n = \frac{r_l \sin(2\mu)}{\sin(\frac{\pi}{2} - \mu)}, \quad (18)$$

where μ can be expressed as

$$\mu = \frac{S - p - d}{2r_l}. \quad (19)$$

We have now derived all the necessary equations to determine α at any state of the C-leg. As a byproduct, we have also solved for n . This leaves us with the task of finding an expression for β , the angle between F_r and F_l .

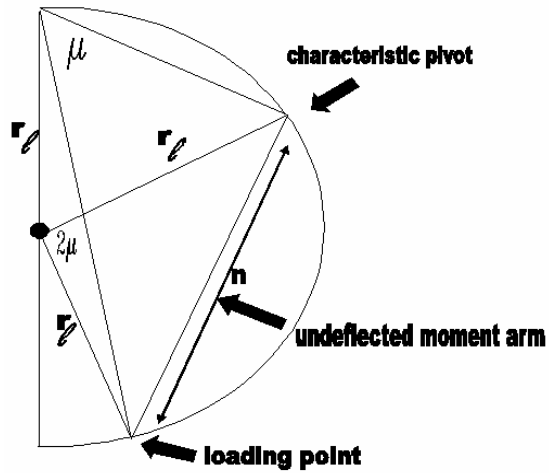


Figure 13: The C-leg as a half-circle with the secants that are relevant to finding n shown.

A simple geometric analysis of *Figure 14*, reveals that

$$\beta = \mu + \varphi. \quad (20)$$

This completes our derivation.

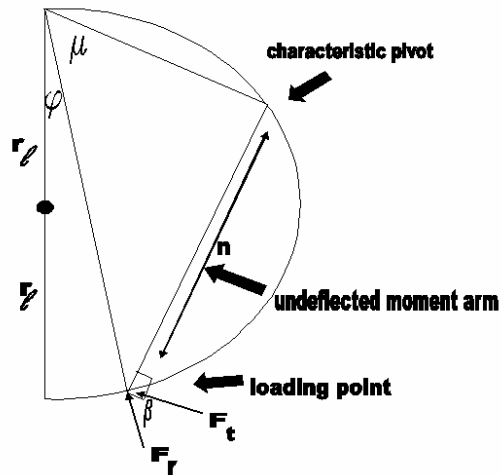


Figure 14: The C-leg as a half-circle with the secants that are relevant to finding β shown.